

Estimation of the Future Distribution of Sea Surface  
Temperature and Sea Ice Using the CMIP3  
Multi-model Ensemble Mean

CMIP3 マルチモデルアンサンブル平均を利用した将来の  
海面水温・海氷分布の推定

Ryo Mizuta<sup>\*1</sup>, Yukimasa Adachi<sup>\*2</sup>, Seiji Yukimoto<sup>\*2</sup> and  
Shoji Kusunoki<sup>\*2</sup>

水田 亮<sup>\*1</sup>・足立 恭将<sup>\*2</sup>・行本 誠史<sup>\*2</sup>・楠 昌司<sup>\*2</sup>

<sup>\*1</sup>*Advanced Earth Science Technology Organization*

地球科学技術総合推進機構

<sup>\*2</sup>*Climate Research Department, Meteorological Research Institute*

気象研究所 気候研究部



## Preface

Future global climate change has been assessed in the Fourth Assessment Report of the Intergovernmental Panel on Climate Change (IPCC-AR4) with higher confidence than in previous reports by using state-of-the-art atmosphere–ocean coupled general circulation models (AOGCM), which have been developed at institutions worldwide and made available under Coupled Model Intercomparison Project phase 3 (CMIP3) as an activity of the World Climate Research Programme (WCRP). The performance of AOGCMs in reproducing historical and present climate has been improved, and the ensemble average of the multi-model results gives the best performance in many aspects.

It has now been recognized that global warming is inevitable unless urgent countermeasures are implemented, and the current emphasis is on the mitigation of the effects of global warming. For this purpose, more precise and detailed information (both spatial and temporal) of future climate change is needed. Such information can be obtained most effectively from atmospheric models with much higher resolution than that of the AOGCMs used for long-term projection. Bottom boundary data (sea surface temperature and sea ice distribution) for the present and future climate must be specified in such "time-slice" simulations. In time-slice simulations, it is essential for the bottom boundary data to be precise and credible with regard to not only mean climate but also temporal variability.

The mean CMIP3 multi-model result is considered the best choice for the boundary data; however, the simple ensemble mean of multi-model data presents several problems. We developed a technique that incorporates the effects of future climate change along with realistic interannual variability, which is smoothed out by the multi-model mean, while correcting for the climatic biases of each model. This report documents this technique. Processed results from the CMIP3 multi-model data are also presented.

The technique was developed as part of the KAKUSHIN Program "Projection of the Change in Future Weather Extremes Using Super-High-Resolution Atmospheric Models" of the Ministry of Education, Culture, Sports, Science and Technology, Japan, with support from the research fund "Integrated Research on Climate Change Scenarios to Increase Public Awareness and Contribute to the Policy Process, Global Environment Research Fund, Ministry of the Environment (Theme 2: Evaluation of CMIP3 multi-model performances for various phenomena)". We hope that the technique described here will be utilized not only by the program for which it was developed but also in other time-slice experiments to obtain precise and detailed information about future climate change in various regions of the world, because its use will help reduce the uncertainty in the information that stems from the use of inconsistent boundary data.

November 2008

Akio Kitoh  
Director  
Climate Research Department

## 序

気候変動に関する政府間パネル第4次評価報告書(IPCC-AR4)において、世界の研究機関で開発された最新の大気海洋結合モデル(AOGCM)を用いて、これまでの報告書よりも高い信頼性をもって将来の世界的な気候変化が評価された。それに用いられたモデルの結果は、世界気候研究計画(WCRP)の活動の一つである結合モデル比較プロジェクト・フェーズ3(CMIP3)のもとで提供されている。それら AOGCM による過去から現在に至る気候の再現性能は向上してきており、またそれら多くのモデルのアンサンブル平均は多くの観点からも最も良い性能を与えることが示されている。

今や、緊急の対策をしなければ地球温暖化は避けることができないことと認識されている。また、地球温暖化に対し、その影響の緩和策により重点が置かれるようになってきている。このような目的のためには、将来の気候変化に関して(空間的にも時間的にも)より正確かつ詳細な情報が求められる。そのような情報は、長期の予測に用いられる AOGCM よりもむしろ、高解像度の大気モデルを用いる方がより効率的に得ることができる。そのような、いわゆる「タイムスライス」シミュレーションのためには、下部境界条件(海面水温および海氷の分布)が必要とされる。タイムスライス・シミュレーションにとって、その下部境界データは、平均的な気候値だけでなく時間的な変動性についても、正確かつ信頼性の高いものであることが非常に重要な要素となる。

CMIP3 の多数のモデル(マルチモデル)の平均から得られる結果は、その境界データとして最良の選択であると考えられる。しかし、マルチモデルのデータを単純に平均するだけでは、いくつかの問題が生じてくる。そこで我々は、それぞれのモデルのバイアスを補正し、マルチモデルを平均した場合に平滑化されて消えてしまう年々変動を現実的に表現しつつ将来の気候変化の効果を取り入れる手法を開発した。この報告はその手法を記述するものである。また、CMIP3 のマルチモデル・データを用いた処理結果も示すことにする。

この技術開発は、文部科学省 21 世紀気候変動予測革新プログラム「超高解像度大気モデルによる将来の極端現象の変化予測に関する研究」の推進に資するために行ったものである。また一部は、環境省地球環境研究総合推進費「地球温暖化に係る政策支援と普及啓発のための気候変動シナリオに関する総合的研究(テーマ2:マルチ気候モデルにおける諸現象の再現性比較とその将来変化に関する研究)」の支援も得た。我々は、それにとどまらず、世界の各地域における将来の気候変化についての正確かつ詳細な情報を得るために、これらのデータが多くのタイムスライス実験に利用されることを願っている。そのように利用されることにより、ばらばらな境界条件データを用いる場合に比べ、不確実性の低減に結びつくものとする。

平成 20 年 11 月

気候研究部長  
鬼頭 昭雄

## Abstract

We estimated future distributions of sea surface temperature, sea ice concentration, and sea ice thickness by using Coupled Model Intercomparison Project phase 3 (CMIP3) multi-model ensemble data for the lower boundary conditions of atmospheric time-slice experiments. The estimation method includes corrections for the present-day climate bias in the model relative to the observation data set and future changes in the multi-model ensemble mean, while keeping the same interannual variability as found in the observation data. These estimated sea surface temperature and sea ice data are useful for simulating, using high-resolution atmospheric models, the most likely effects of future climate change on small-scale atmospheric phenomena, under the assumptions that oceanic variability is unchanged in the mean future climate and that atmosphere–ocean interaction is negligible.

## 概要

結合モデル比較プロジェクト・フェーズ3 (CMIP3) マルチモデルアンサンブル平均を利用して、将来の海面水温と海氷の分布を推定し、大気モデルによるタイムスライス実験で下部境界条件として用いる方法を考案した。この方法は、観測された年々変動をそのまま用いながら、観測に対するモデルの現在気候のバイアスの補正と、マルチモデルアンサンブルで表現される将来変化の効果を含んだものとなっている。この分布は、海洋の変動が将来気候においても変化せず大気海洋相互作用が無視できるという仮定の下で高解像度の大気モデルでを使用することにより、もっとも起こりうる将来の気候変化影響をシミュレートするのに有用である。

# Contents

1. Introduction	.....	1
2. Methods	.....	2
2.1 Sea surface temperature	.....	2
2.2 Sea ice concentrations	.....	4
2.3 Sea ice thickness	.....	6
3. Verification of the estimated distributions	.....	8
4. Discussion	.....	10
Acknowledgements	.....	11
References	.....	11
Supplementary Information	.....	13



## 1. Introduction

Climate experiments with atmospheric general circulation models (AGCM) using prescribed sea surface boundary conditions are called "time-slice" experiments, and they require horizontal distribution data for sea surface temperature (SST) and sea ice concentration and thickness. Although we can use observation data sets for present-day climate experiments (AMIP-type experiments), data from atmosphere–ocean coupled general circulation models (CGCM) are often used for experiments simulating the future climate, such as that during several decades after the present or during the last decades of the 21st century. However, when we conduct a future-climate experiment by using an AGCM to evaluate possible future changes, the direct use of a CGCM's output for future boundary conditions gives rise to various problems as follows:

1. Because a CGCM's output for the present-day climate shows some bias when compared with observation data, it is difficult to evaluate future changes simply by taking the difference between AGCM results obtained by using the observed conditions and those obtained by using the output of a CGCM for future conditions.

2. By using the present-day output of a CGCM for the AGCM present-day conditions as well as for experiments on future conditions, we can evaluate future changes by taking the difference between the two results. However, it is difficult to obtain a good representation of the present-day climate with the AGCM because of the bias in the CGCM.

3. The use of the multi-model ensemble mean (MEM) of many CGCMs for the AGCM present-day and the AGCM future conditions can cancel much of the bias of the individual models and can reduce the uncertainty in the simulated future changes, but it also cancel the interannual variability in the results of the individual models.

Therefore, it is appropriate to embed the changes from the present-day to the future in the CGCM results in the observation data and then to use those data for the AGCM simulation of future conditions, to compare with the AGCM results obtained using the observed conditions. However, the simple superposition of the changes in the observation data is problematic because the trend and interannual variability in the obtained data introduce inconsistency. This occurs especially near the ice edge, since the location of the ice edge, where future changes of sea ice are largest, differs between in the CGCM results and the observation data. As a result, the future retreat of the sea ice is not represented appropriately as described later.

In this work, we present a method for estimating the future distributions of SST and sea ice that avoids these problems by decomposing the observation data and the CGCM outputs into long-term mean, linear trend, and interannual variability, and then combining some of these components. Changes in the sea ice extent in each hemisphere are taken into account in the estimation of sea ice

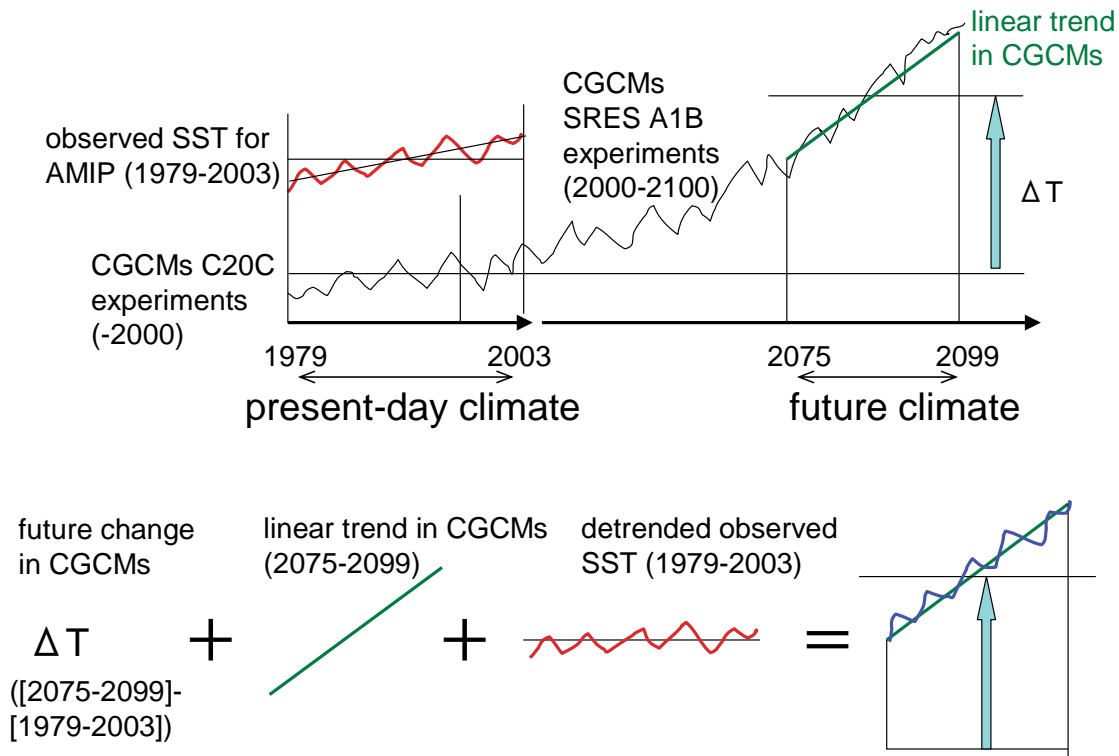


**Fig. 1:** The method used for estimating future SSTs.

concentrations. By using the estimated distributions of SST and sea ice for the lower boundary conditions in the AGCM experiment on future conditions and using the observed conditions for the AGCM present-day experiment, we can use the difference between the two results to represent the effect of climate change caused by the lower boundary condition changes. By also including increases in greenhouse gases and other effects in the experiments simulating future conditions, we can simulate the changes that are most likely to happen in the future.

## 2. Methods

### 2.1 Sea surface temperature

After calculating the MEMs of the CGCMs, the MEM and observation SSTs are decomposed into three terms as follows:

$$\begin{aligned}
 SST_{\text{obs}}(y_1, m, x) &= SST_{\text{obs}_A}(m, x) + SST_{\text{obs}_T}(y_1, m, x) + SST_{\text{obs}_V}(y_1, m, x), \\
 SST_{\text{mp}}(y_1, m, x) &= SST_{\text{mp}_A}(m, x) + SST_{\text{mp}_T}(y_1, m, x) + SST_{\text{mp}_V}(y_1, m, x), \\
 SST_{\text{mf}}(y_2, m, x) &= SST_{\text{mf}_A}(m, x) + SST_{\text{mf}_T}(y_2, m, x) + SST_{\text{mf}_V}(y_2, m, x),
 \end{aligned} \tag{1}$$

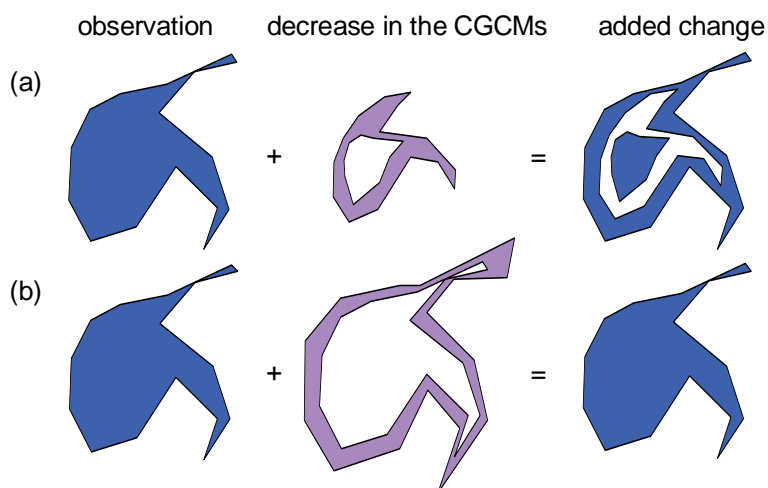


**Fig. 2:** Inconsistencies that can arise in the sea ice distribution when the difference between the present-day and future conditions in the CGCM results (center) is simply added to the observation data (left), when the ice edge of the CGCM is located within the observational ice edge (a), or when the MEMM ice edge is located outside the observational ice edge (b).

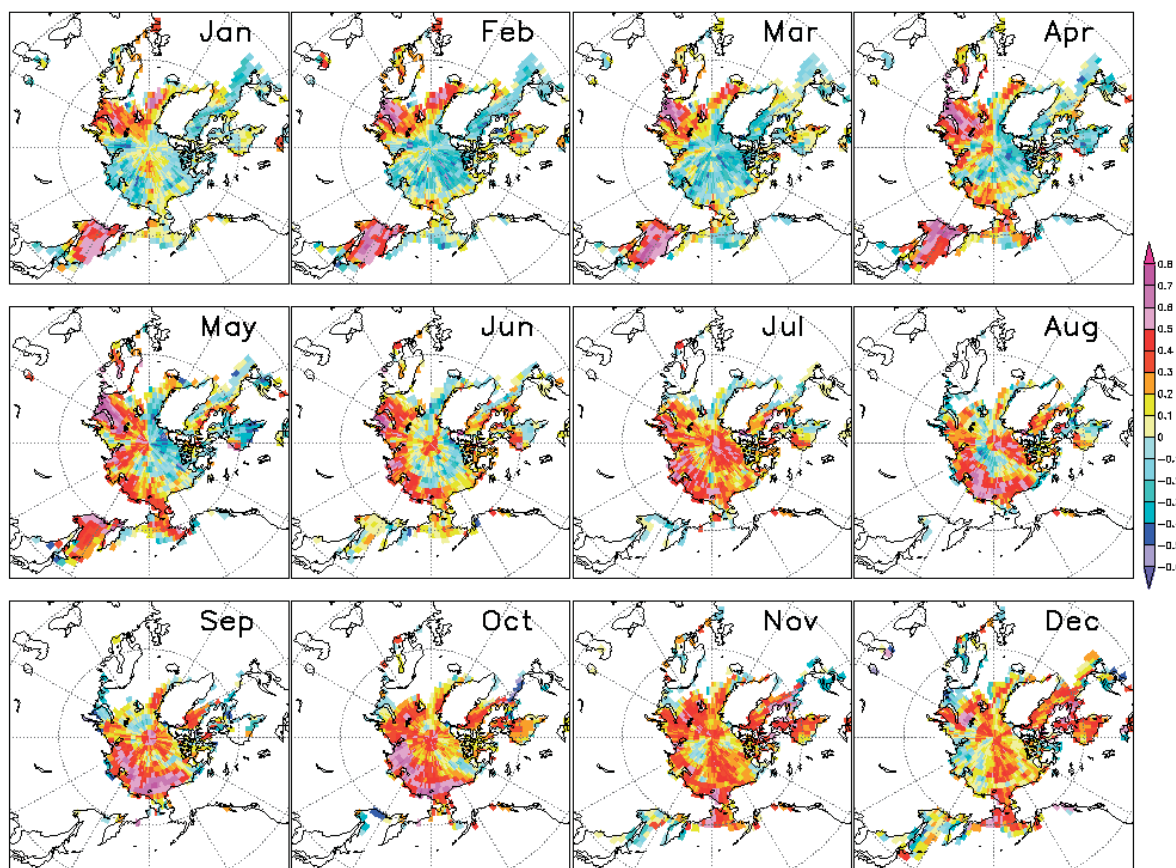


**Fig. 3:** Correlation coefficients between the sea ice extent in the Northern Hemisphere and the sea ice concentration at each grid point.

where obs is the observation data; mp and mf are the MMEMs for the present-day and future climate, respectively; A indicates the long-term mean; T indicates the linear trend; and V refers to the interannual variability, which is defined as the residual of A and T. Decomposition is performed at every grid point  $x$  for every month  $m$  of every year, with  $y_1$  indicating present-day years and  $y_2$  indicating future years.

The values of future distributions,  $SST_{\text{future}}$ , are estimated as follows:

$$SST_{\text{future}}(y_2, m, x) \equiv SST_{\text{obs\_A}}(m, x) + (SST_{\text{mf\_A}}(m, x) - SST_{\text{mp\_A}}(m, x)) + SST_{\text{mf\_T}}(y_2, m, x) + SST_{\text{obs\_V}}(y_1, m, x). \quad (2)$$

The difference between the mean present-day and future values simulated in CGCMs is a crucial component of climate change, so it is added to the observed mean to represent the estimated long-term mean. The trend in the MMEM is used as the estimated future trend. For the interannual variability, the observed variability is used as the estimated variability, under the assumption that the variability will not change in the future, because  $SST_{\text{mp\_V}}$  and  $SST_{\text{mf\_V}}$  are both very small owing to the cancellation of individual model variabilities. For each  $y_2$ ,  $y_1$  is chosen so that  $y_2 - y_1$  is a constant value, as described in Section 3. A schematic diagram of this estimation method is presented in Figure 1.

## 2.2 Sea ice concentrations

If the future distribution of sea ice concentration,  $f_{\text{ice}}(y_2, m, x)$ , is estimated by the same method as the SST, it is highly likely that some inconsistencies will occur near the ice edge, as shown in Figure 2. This inconsistency occurs when the location of the ice edge, where the sea ice changes are largest, differs between the CGCM results and observation data. When the MMEM ice edge is located within the observational ice edge, the largest ice change also occurs within the observational ice edge. Adding the change to the observation data makes the distribution non-monotonic in the meridional direction (Fig. 2a). On the other hand, when the ice edge of the MMEM is outside the observational ice edge, little or no ice change occurs within the observational ice edge. Therefore, when the change is added to the observation data, no sea ice retreat as a result of climate change is represented (Fig. 2b).

Because the change that most affects the AGCM results is the change in the sea ice area extent, it is desirable for the change of sea ice extent between the observation data and the estimated future to be the same as the change from the CGCM present to the CGCM future. The correlations between the sea ice extent in the Northern Hemisphere and the sea ice concentration at each grid point (Fig. 3) are high, except in the center of the ice cap, where variability is small. Therefore, the sea ice concentration  $f_{\text{ice}}(y_2, m, x)$  in the future can be estimated from the change in the sea ice extent in each hemisphere as follows (Fig. 4):

1. In each hemisphere, the sea ice extent,  $S_{\text{ice}}$ , is defined as a function of the sea ice concentration  $f$ ,

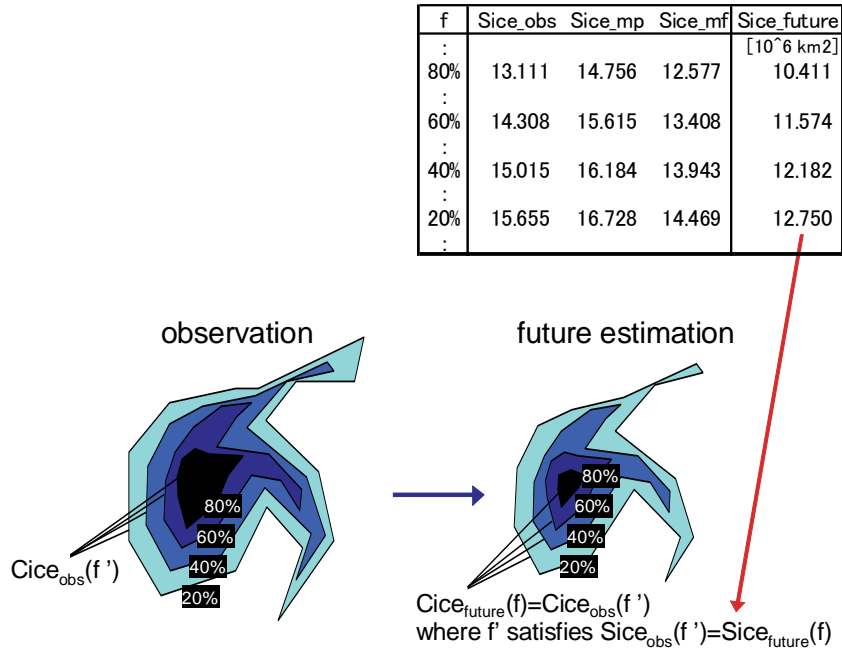


**Fig. 4:** Diagram of the method used for estimating future sea ice concentrations.  $Sice_{obs}$ ,  $Sice_{mp}$ , and  $Sice_{mf}$  are functions of  $f$ . The example values in the table (top) are for  $y_1 = 1994$ ,  $y_2 = 2090$ , and  $m = 3$  in the Northern Hemisphere. (bottom) The correspondence between  $Cice_{obs}(y_1, m, h, f)$ , and  $Cice_{future}(y_2, m, h, f)$ .

so that  $Sice(f)$  is the area in which the concentration is more than  $f$ . The extent in every month  $m$  of every year  $y$  is calculated separately for each hemisphere  $h$ .

2. The sea ice extent in the future is estimated in the same way as SST (Eq. 2) by using the monthly sea ice extent,  $Sice$ :

$$\begin{aligned}
 Sice_{future}(y_2, m, h, f) \equiv & Sice_{obs\_A}(m, h, f) + (Sice_{mf\_A}(m, h, f) - Sice_{mp\_A}(m, h, f)) \\
 & + Sice_{mf\_T}(y_2, m, h, f) + Sice_{obs\_V}(y_1, m, h, f).
 \end{aligned} \quad (3)$$

3. For each month,  $fice_{future}(y_2, m, x)$  in the future is estimated by shrinking the observed extent,  $fice_{obs}(y_1, m, x)$ , while keeping the shape of the ice cap, until  $Sice_{future}(y_2, m, h, f)$  is equal to Eq. (3). To do so, we prepare the isopleth shapes  $Cice_{obs}(y_1, m, h, f)$  as a function of  $f$  for the observed sea ice distribution (Fig. 4, left), obtaining the correspondence between  $f$ ,  $Sice_{obs}(y_1, m, h, f)$ , and  $Cice_{obs}(y_1, m, h, f)$ . Next, we find  $f'$  for each  $f$  that satisfies

$$Sice_{obs}(y_1, m, h, f') = Sice_{future}(y_2, m, h, f). \quad (4)$$

Then, the isopleth  $f$  in the future is estimated by

$$Cice_{future}(y_2, m, h, f) \equiv Cice_{obs}(y_1, m, h, f'). \quad (5)$$

By combining  $Cice_{future}(y_2, m, h, f)$  estimated for  $f$  from 0% to 100%, we can obtain the estimated distribution of sea ice concentrations in the future.

### 2.3 Sea ice thickness

The sea ice thickness in the future is estimated so that the rate of change in the sea ice volume is equal to the rate of change in the MEMM results. For simplicity, the estimated thickness distribution  $dice_{future}(m, x)$  defined for each month is obtained by multiplying the observed thickness distribution by a constant  $\alpha$ :

$$dice_{future}(m, x) \equiv \alpha \cdot dice_{obs}(m, x). \quad (6)$$

Here, since we have only the climatology of the thickness observations and do not have reliable observed trends or interannual variability, we use a future thickness distribution that has only seasonal variation and no interannual variability.

The constant  $\alpha$  is obtained as follows (Fig. 5). First, the sea ice volume,  $Vice$ , in each hemisphere for the observation data and the MEMM is calculated:

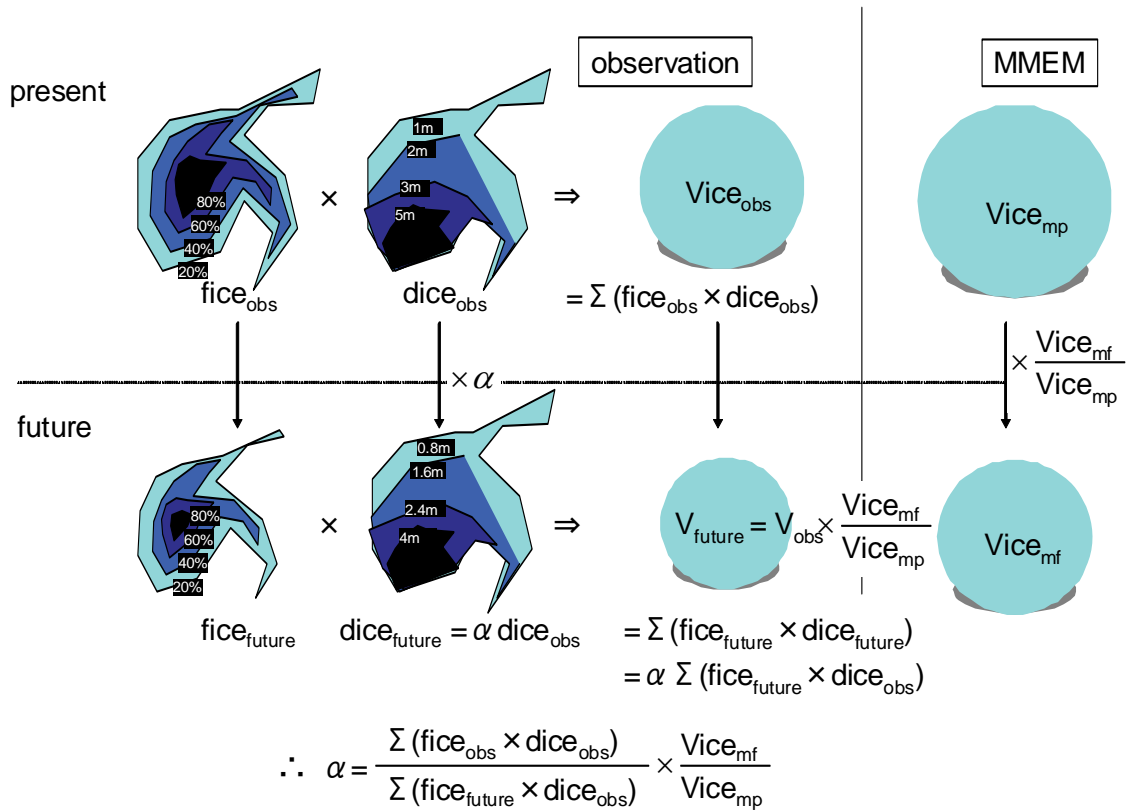


**Fig. 5:** Diagram of the method used for estimating future sea ice thickness.

$$\begin{aligned}
 Vice_{\text{obs}}(m, h) &= \sum_{x, y1} \{fice_{\text{obs}}(y_1, m, x) \times dice_{\text{obs}}(m, x)\}, \\
 Vice_{\text{mp}}(m, h) &= \sum_{x, y1} \{fice_{\text{mp}}(y_1, m, x) \times dice_{\text{mp}}(y_1, m, x)\}, \\
 Vice_{\text{mf}}(m, h) &= \sum_{x, y2} \{fice_{\text{mf}}(y_2, m, x) \times dice_{\text{mf}}(y_2, m, x)\}.
 \end{aligned} \tag{7}$$

Sea ice volume  $Vice_{\text{future}}(m, h)$  in the future is estimated so that the rate of change from the observation data is equal to the rate of change in the MMEM results:

$$Vice_{\text{future}}(m, h) \equiv Vice_{\text{obs}}(m, h) \times \frac{Vice_{\text{mf}}(m, h)}{Vice_{\text{mp}}(m, h)}. \tag{8}$$

Since

$$\begin{aligned}
 Vice_{\text{future}}(m, h) &= \sum_{x, y2} \{fice_{\text{future}}(y_2, m, x) \times dice_{\text{future}}(m, x)\} \\
 &= \sum_{x, y2} \{fice_{\text{future}}(y_2, m, x) \times \alpha dice_{\text{obs}}(m, x)\} \\
 &= \alpha \sum_{x, y2} \{fice_{\text{future}}(y_2, m, x) \times dice_{\text{obs}}(m, x)\},
 \end{aligned} \tag{9}$$

$\alpha$  can be calculated by

$$\alpha = \frac{\sum_{x, y1} \{fice_{\text{obs}}(y_1, m, x) \times dice_{\text{obs}}(m, x)\}}{\sum_{x, y2} \{fice_{\text{future}}(y_2, m, x) \times dice_{\text{obs}}(m, x)\}} \times \frac{Vice_{\text{mf}}(m, h)}{Vice_{\text{mp}}(m, h)}. \tag{10}$$

**Table 1:** Data sets used for the CMIP3 models.

Name	Institute
bccr_bcm2_0	Bjerknes Centre for Climate Research, Norway
cccma_cgcm3_1	Canadian Centre for Climate Modeling & Analysis, Canada
cccma_cgcm3_1_t63	
cnrm_cm3	Météo-France/Centre National de Recherches Météorologiques, France
csiro_mk3_0	CSIRO Atmospheric Research, Australia
gfdl_cm2_0	U.S. Dept. of Commerce/NOAA/Geophysical Fluid Dynamics Laboratory,
gfdl_cm2_1	USA
giss_aom	NASA/Goddard Institute for Space Studies, USA
inmcm3_0	Institute for Numerical Mathematics, Russia
ipsl_cm4	Institut Pierre Simon Laplace, France
miroc3_2_hires	Center for Climate System Research (University of Tokyo), National
miroc3_2_medres	Institute for Environmental Studies, and Frontier Research Center for Global Change (JAMSTEC), Japan
miub_echo_g	Meteorological Institute of the University of Bonn, Meteorological Research Institute of KMA, and Model & Data Group, Germany/Korea
mpi_echam5	Max Planck Institute for Meteorology, Germany
mri_cgcm2_3_2a	Meteorological Research Institute, Japan
ncar_ccsm3_0	National Center for Atmospheric Research, USA
ukmo_hadcm3	Hadley Centre for Climate Prediction and Research/Met Office, UK
ukmo_hadgem1	

### 3. Verification of the estimated distributions

We estimated the distributions for 2015–2039 and 2075–2099 by this method using the observation data and the MEMM. Monthly mean data from the Hadley Center (Rayner et al., 2003) from 1979 to 2003 were used for the observed SST and sea ice concentration data, along with the monthly climatology of sea ice thickness from Bourke and Garrett (1987). The results of the Climate of the Twentieth Century Project (C20C) experiments (until 2000) and the SRES A1B scenario experiments (after 2000) of 18 CMIP3 CGCMs (Meehl et al. 2007) were used for the MEMM. The CGCMs used here are listed in Table 1. We used only one experiment from models with multiple experiments. Phases of the observed interannual variability  $SST_{obs\_y}$  during  $y_1 = 1979, \dots, 2003$  were shifted 36 or

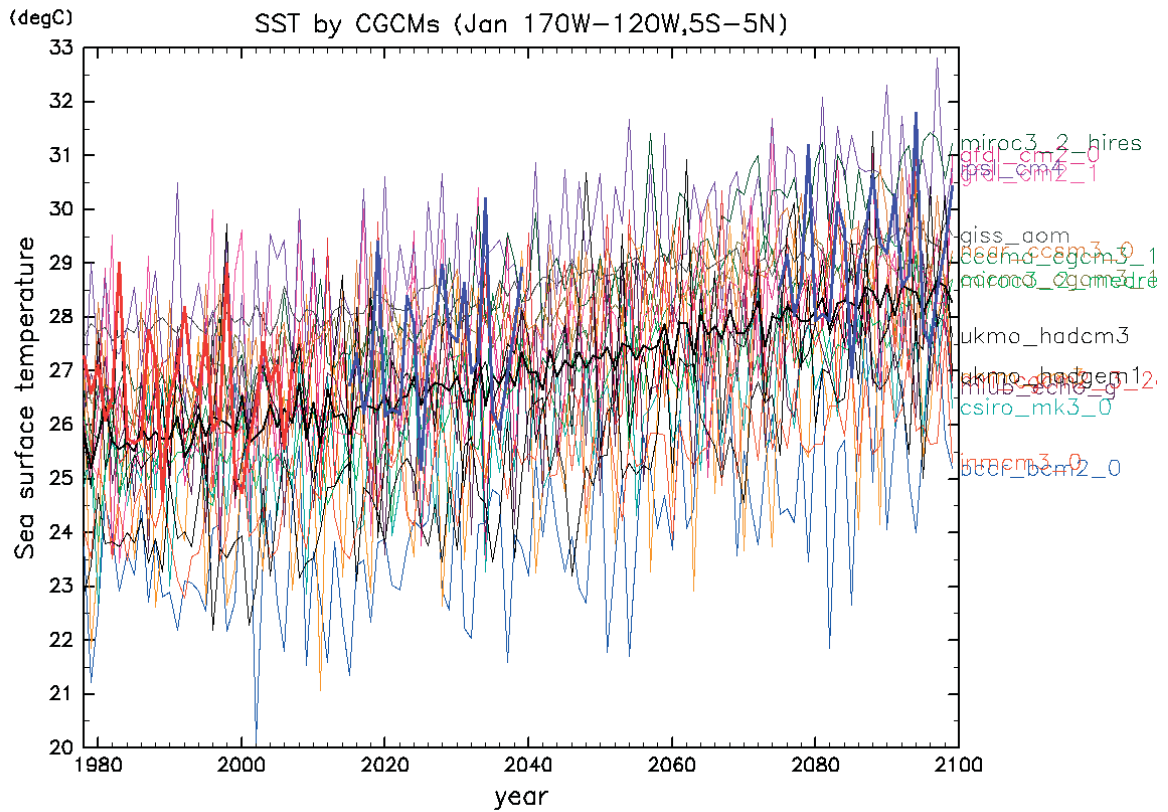


**Fig. 6:** Sea surface temperatures averaged over 170°W–120°W and 5°S–5°N in January. Thin lines are the CGCM results, and the thick black line is the ensemble mean of the CGCM results. The thick red line is the observation data, and the thick blue lines denote  $SST_{\text{future}}$ , estimated by Eq. (2) for 2015–2039 and 2075–2099.

96 years to  $y_2 = 2015, \dots, 2039$  or  $y_2 = 2075, \dots, 2099$  for use in Eqs. (2) and (3). For example,  $y_1 = 1979$  was used with  $y_2 = 2015$  or  $y_2 = 2075$ , and  $y_1 = 1980$  was used with  $y_2 = 2016$  or  $y_2 = 2076$ . This same correspondence between  $y_1$  and  $y_2$  was also used when shrinking the sea ice distribution (Eqs. (4) and (5)). In Eq. (5), we calculated  $Cice_{\text{future}}(y_2, m, h, f)$  for  $f$  with intervals of 0.1%.

Figure 6 shows SST averaged over the tropical Pacific region in the observation data, the CGCMs, the MMEM, and the estimated future. The variability in this region is mainly due to ENSO. Although each CGCM (thin colored lines) shows more or less interannual variability, the MMEM (thick black line) shows very small variability because of cancellation of variation phases. Since the observed SST (thick red line) is higher than the MMEM by about 0.7 K, the estimated SST (thick blue lines) obtained by Eq. (2) is also higher than the MMEM.

Figure 7 shows Northern Hemisphere sea ice concentrations in March during three observation years ( $y_1 = 1994, 1998,$  and  $2002$ ), and estimated concentrations in three future years ( $y_2 = 2090, 2094,$  and  $2098$ ). In the future estimations, sea ice decreases and retreats around Newfoundland and the Sea of

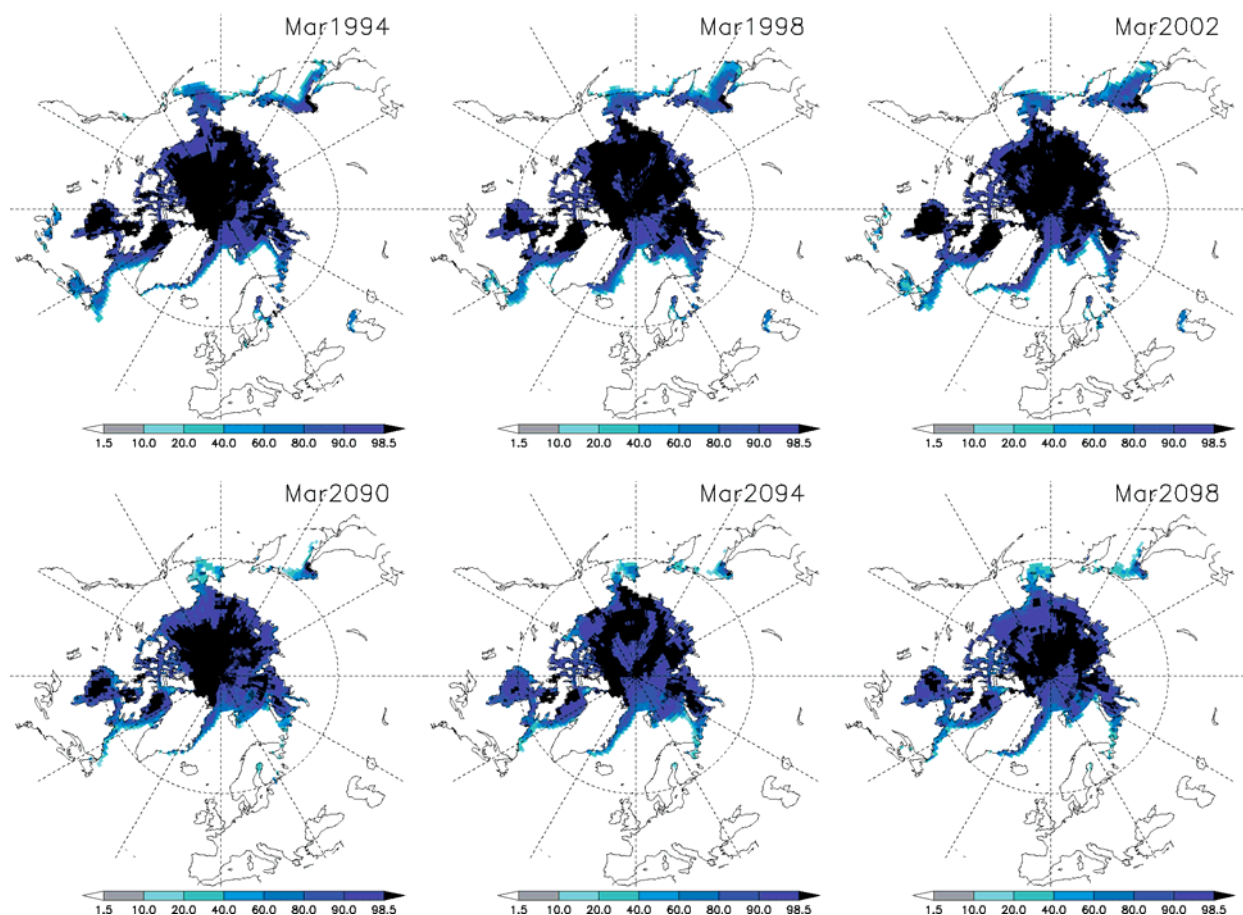


**Fig. 7:** Horizontal distributions of sea ice concentrations in March in the observation data,  $fice_{\text{obs}}(y_1, m, x)$  (top), and estimated  $fice_{\text{future}}(y_2, m, x)$  in the future (bottom).

Okhotsk. Some interannual variability in the observation data is apparent: in 1994, more sea ice was observed in the Western Hemisphere, and in 1998, more was observed in the Eastern Hemisphere. This kind of variability is kept in the estimated distribution: There is more sea ice in the Western Hemisphere in 2090 and more in the Eastern Hemisphere in 2094, because in Eq. (5) the sea ice distribution in  $y_2$  is calculated using the isopleths of the sea ice concentration in  $y_1$ .

As supplemental information, monthly SST, sea ice concentration, and sea ice thickness and their changes averaged over the 25 years, along with monthly  $SST_{\text{mf}_T}$  and  $SST_{\text{obs}_V}$ , are shown in Figs. S1–S16.

#### 4. Discussion

There is large uncertainty with regard to the future changes in the amplitude and horizontal pattern of interannual variability. A variety of changes in ENSO are found in CMIP3 CGCMs (IPCC 2007). Whereas a linear trend induced by the greenhouse gas increase is dominant in the linear trend of the

MMEM future experiments, that is not the case in the present-day climate (either in the observation data or the MMEM present experiments). Decadal variability accounts for the calculated linear trend in the present-day climate to a certain degree, mainly because of the short time period of the data. In this work, therefore, we used observation data alone for estimating future interannual variability, and MMEM future results alone for estimating the future linear trend. Correction of the bias in the linear trend between the MMEM present and the observation data might be desirable if the effect of decadal variability could be removed from the calculated linear trend.

If we take the median sea ice concentration of the present-day CGCM experiments, a distribution very similar to the observation data is obtained. Thus, it would be possible to estimate the long-term mean of the locations of future decreases by calculating  $fice_{mf} - fice_{mp}$ . However, interannual variability in the location of the decrease is not represented in such a calculation because interannual variability in MMEM is very small as a result of cancellations.

The estimated SST, sea ice concentration, and sea ice thickness have been used as boundary conditions in simulations of an AGCM with a horizontal grid size of 20 km performed by the Earth Simulator. Although the method described in this work would have difficulty estimating values for the very near future, when the phases of the interannual variation would be continuous with the present-day observation data, it is nevertheless one of the most objective methods available by which to estimate sea surface conditions 10 to 100 years from now by using the MMEM results.

### Supplementary Information

Monthly SST, sea ice concentration, and sea ice thickness, their changes averaged over the 25 years, and monthly  $SST_{mf\_T}$  and  $SST_{obs\_V}$ , are shown in Supplemental Figs. S1–S16.

### Acknowledgements

This work was supported by the "Projection of Change in Future Weather Extremes Using Super-High-Resolution Atmospheric Models" project as a part of the KAKUSHIN Program of the Ministry of Education, Culture, Sports, Science and Technology of Japan, and by the Global Environment Research Fund (S-5-2) of the Ministry of the Environment of Japan.

### References

- Bourke, R.H. and R.P. Garrett, 1987: Sea ice thickness distribution in the Arctic Ocean. *Cold Regions Sci. and Tech.*, **13**, 259-280.
- Intergovernmental Panel on Climate Change, 2007: Climate change 2007: The Physical Science Basis—Contribution of the Working Group I to the Fourth Assessment Report of the

Intergovernmental Panel on Climate Change, Cambridge Univ. Press, Cambridge, U. K., 996pp.

Meehl, G., C. Covey, T. Delworth, M. Latif, B. McAvaney, J. Mitchell, R. Stouffer, and K. Taylor, 2007: The WCRP CMIP3 multimodel dataset: A new era in climate change research. *Bull. Am. Meteorol. Soc.*, **88**, 1383–1394.

Rayner, N. A., D. E. Parker, E. B. Horton, C. K. Folland, L. V. Alexander, D. P. Rowell, E. C. Kent, and A. Kaplan, 2003: Global analyses of sea surface temperature, sea ice, and night marine air temperature since the late nineteenth century. *J. Geophys. Res.*, **108(D14)**, 4407, doi:10.1029/2002JD002670.

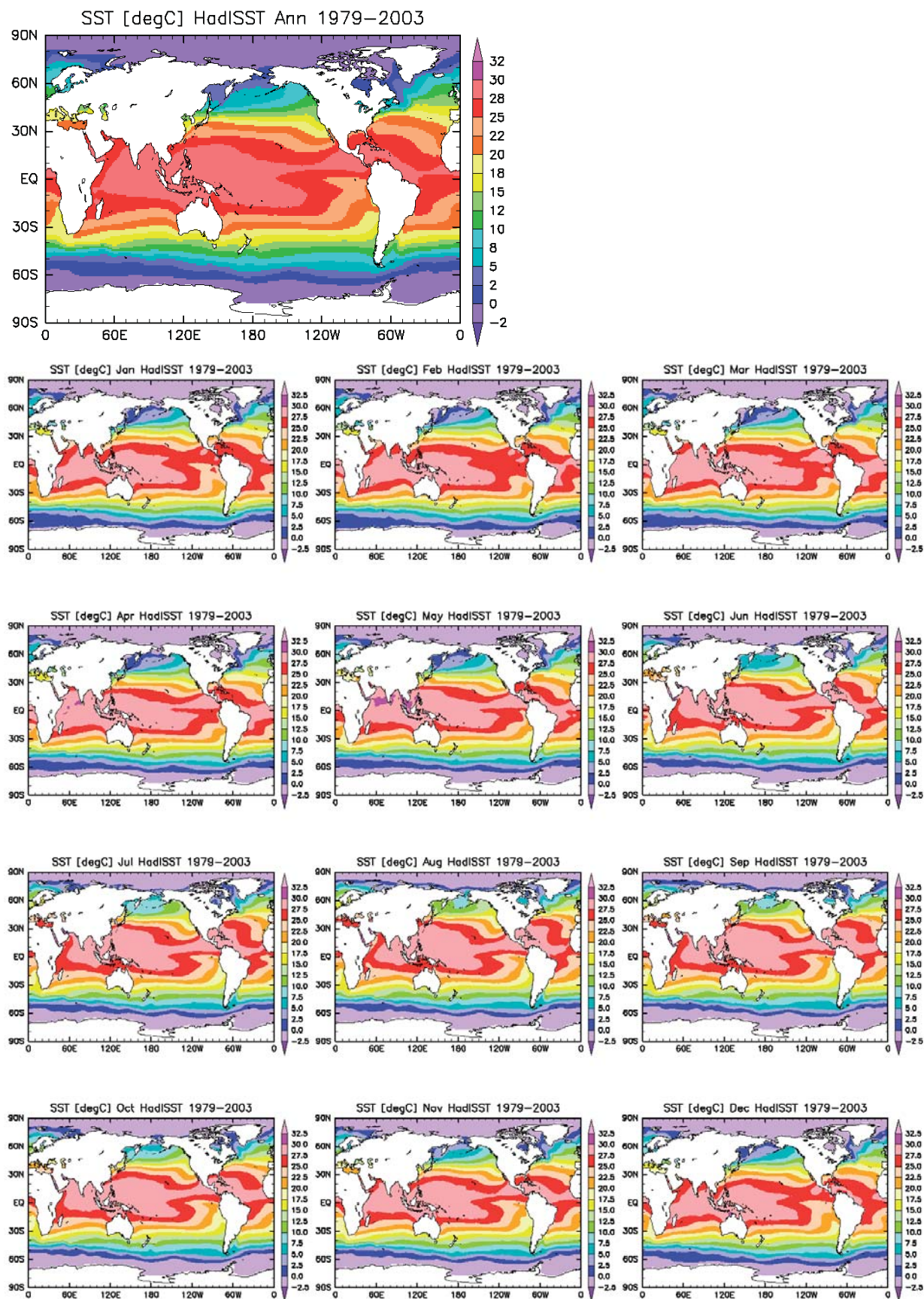


**Fig. S1:** Observational distributions of annual mean SSTs and monthly SSTs averaged from 1979 to 2003.

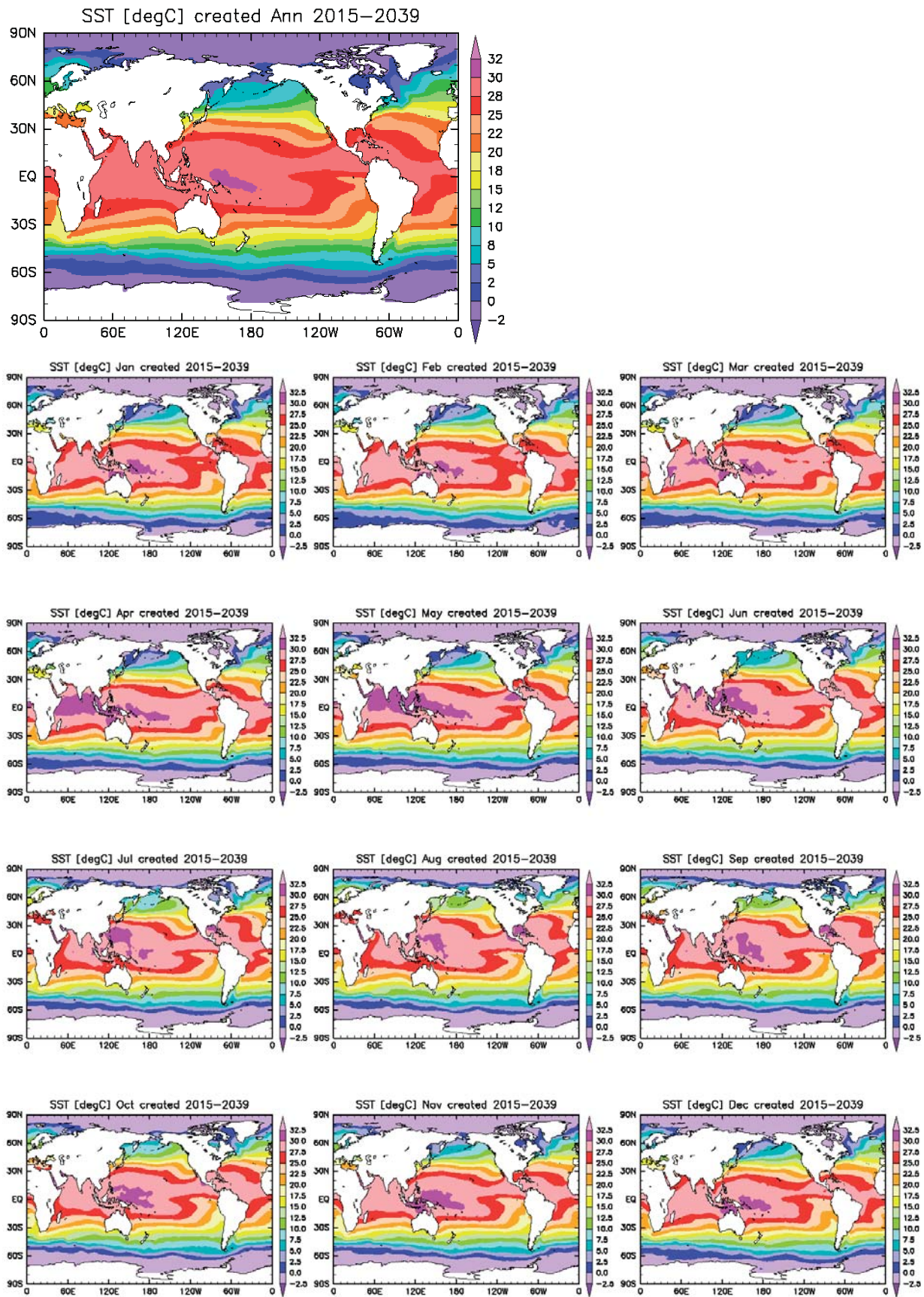


**Fig. S2:** Estimated near-future distributions of annual mean SSTs and monthly SSTs, averaged from 2015 to 2039.

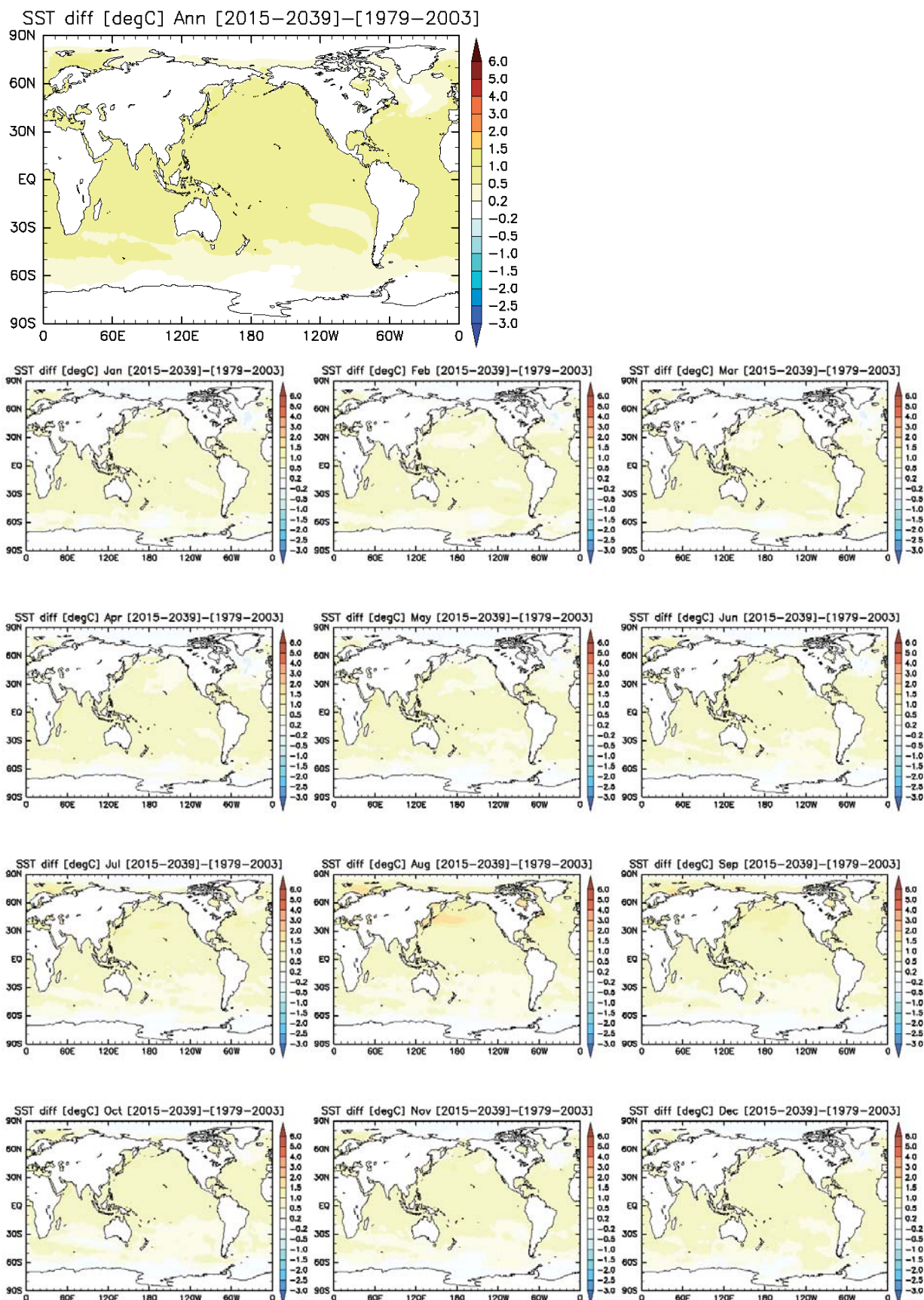


**Fig. S3:** Differences in the annual mean SSTs and monthly SSTs between the observation data (1979–2003) and the estimated near-future values (2015–2039).

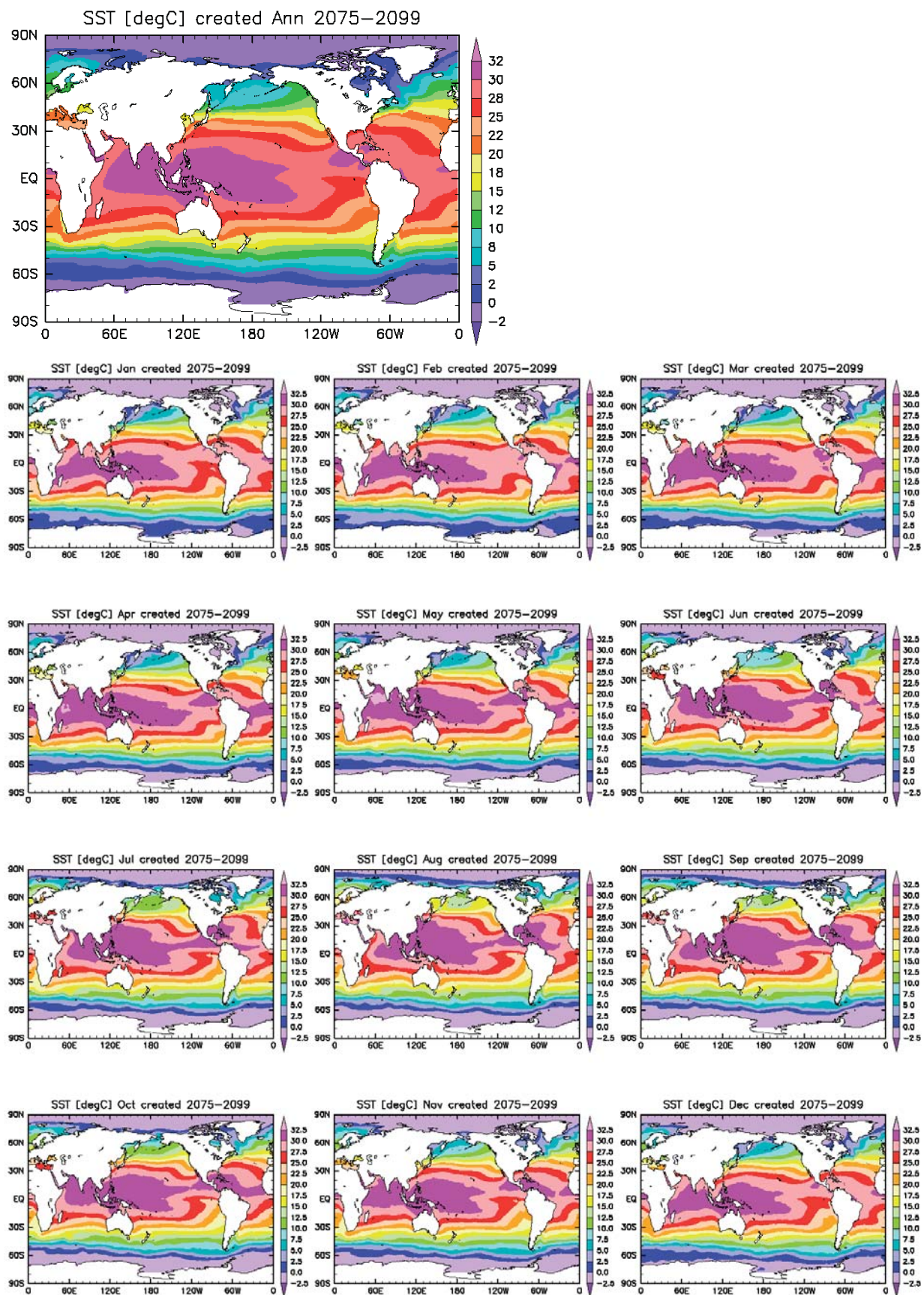


**Fig. S4:** Estimated future distributions of annual mean SSTs and monthly SSTs averaged from 2075 to 2099.

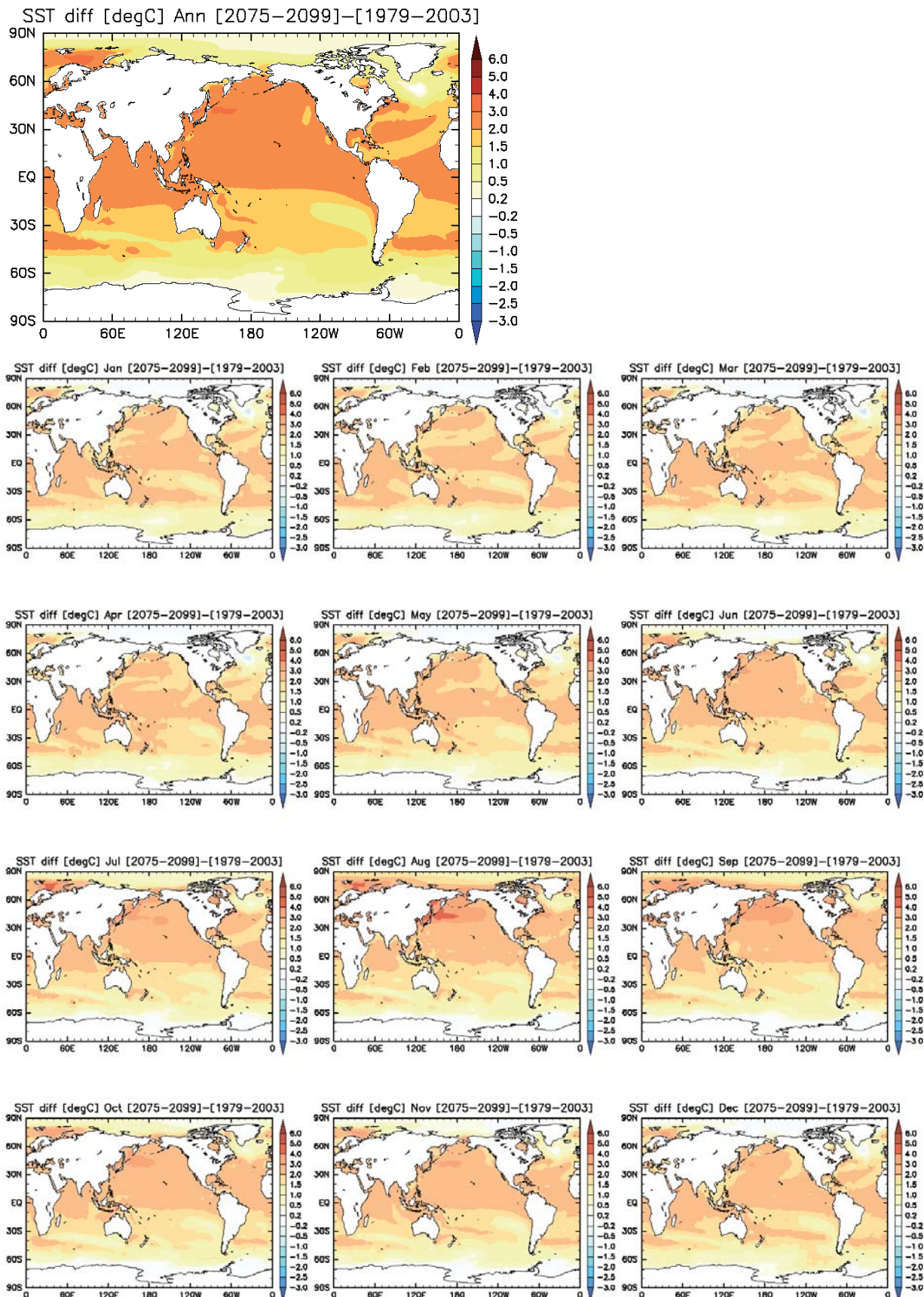


**Fig. S5:** Differences in the annual mean SSTs and monthly SSTs between the observation data (1979–2003) and the estimated future values (2075–2099).

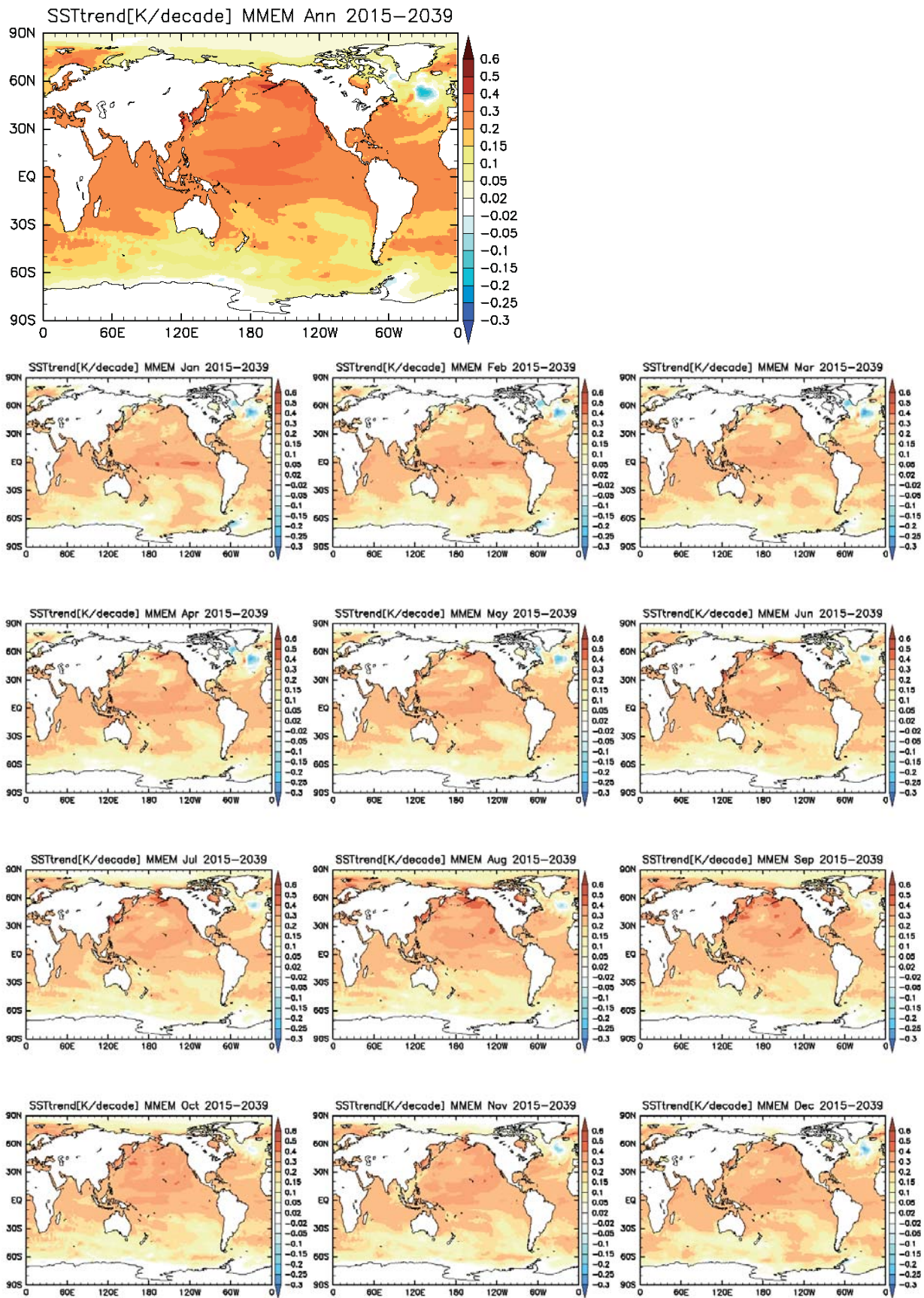


**Fig. S6:** Linear trends in the multi-model ensemble mean SSTs during 2015 to 2039. Units are K/decade.

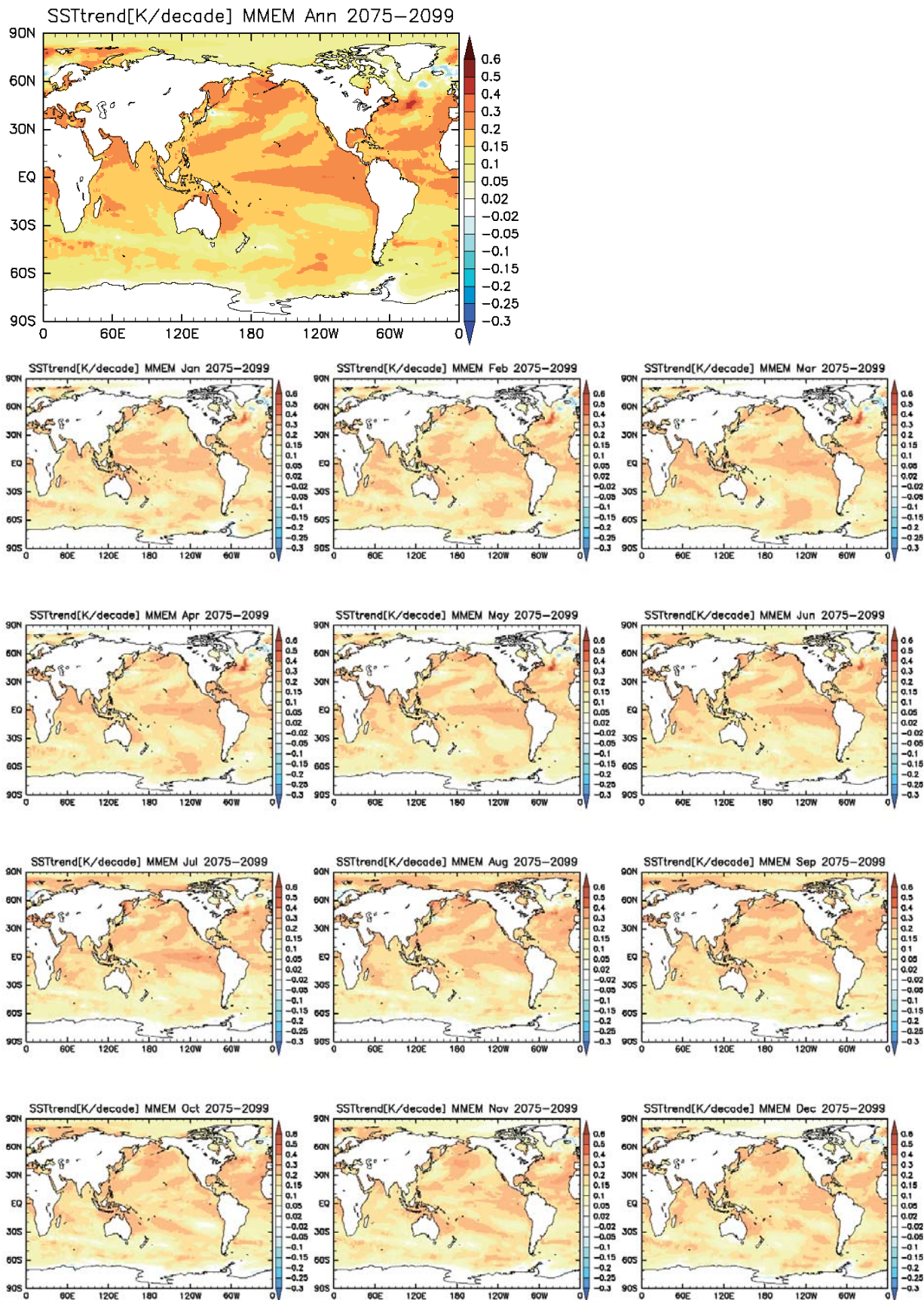


**Fig. S7:** Linear trends in the multi-model ensemble mean SSTs during 2075 to 2099. Units are K/decade.

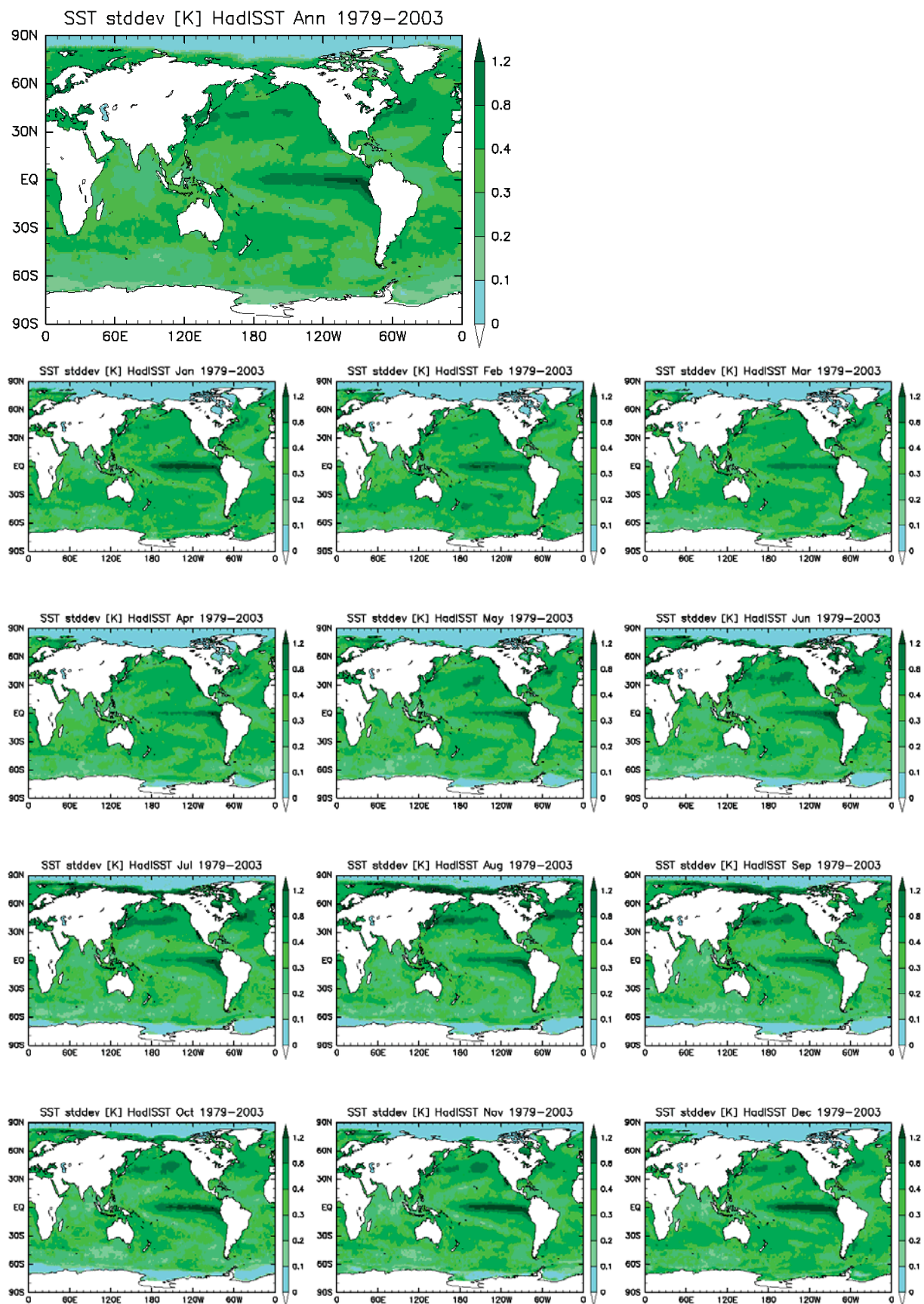


**Fig. S8:** Standard deviations of the interannual variations in the observed SSTs after removing the linear trend during 1979–2003.

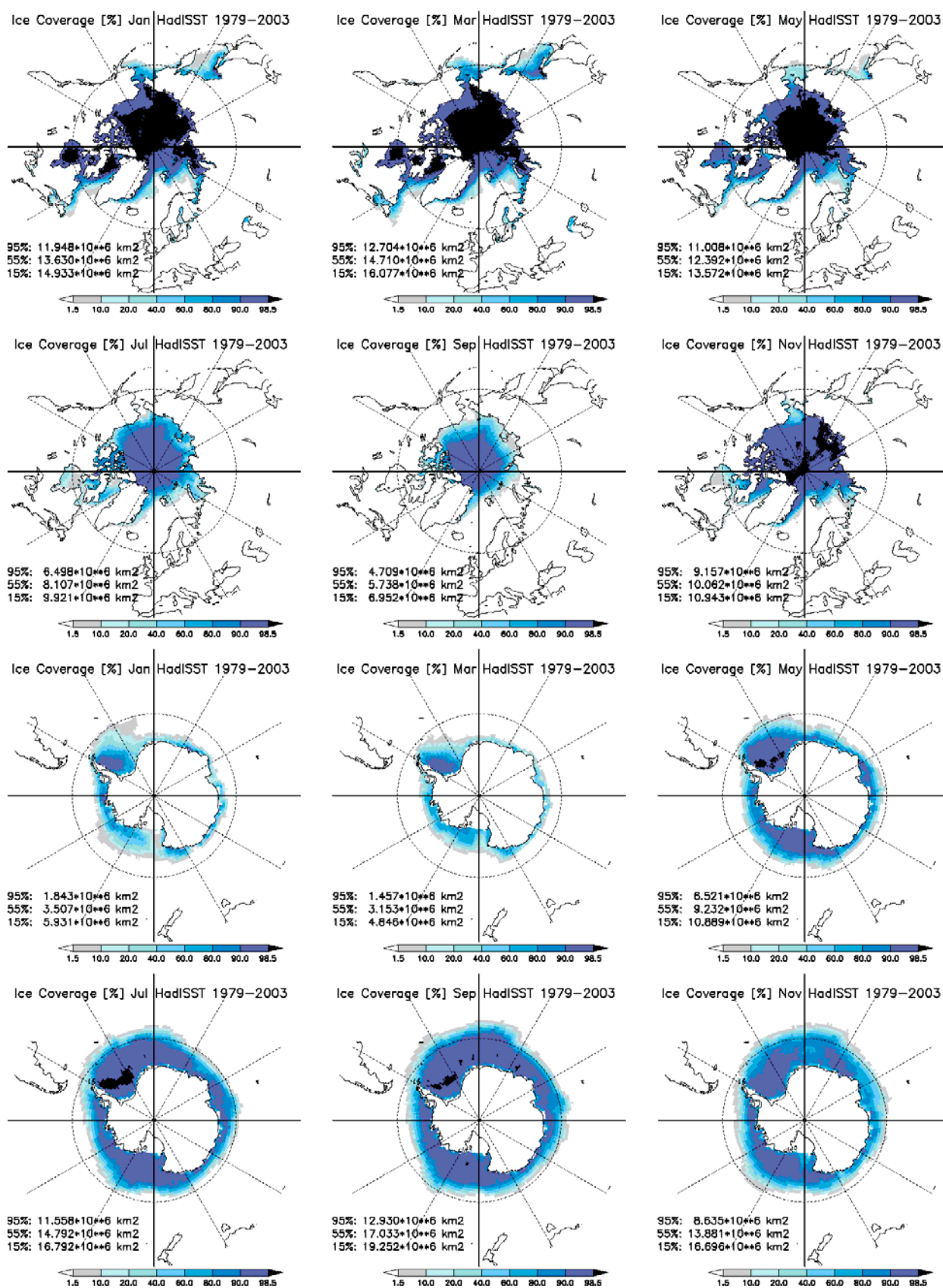


**Fig. S9:** Observational distributions of monthly sea ice concentrations averaged from 1979 to 2003. The values in the figure denote the sea ice extent for  $f=95\%$ ,  $55\%$ , and  $15\%$ .

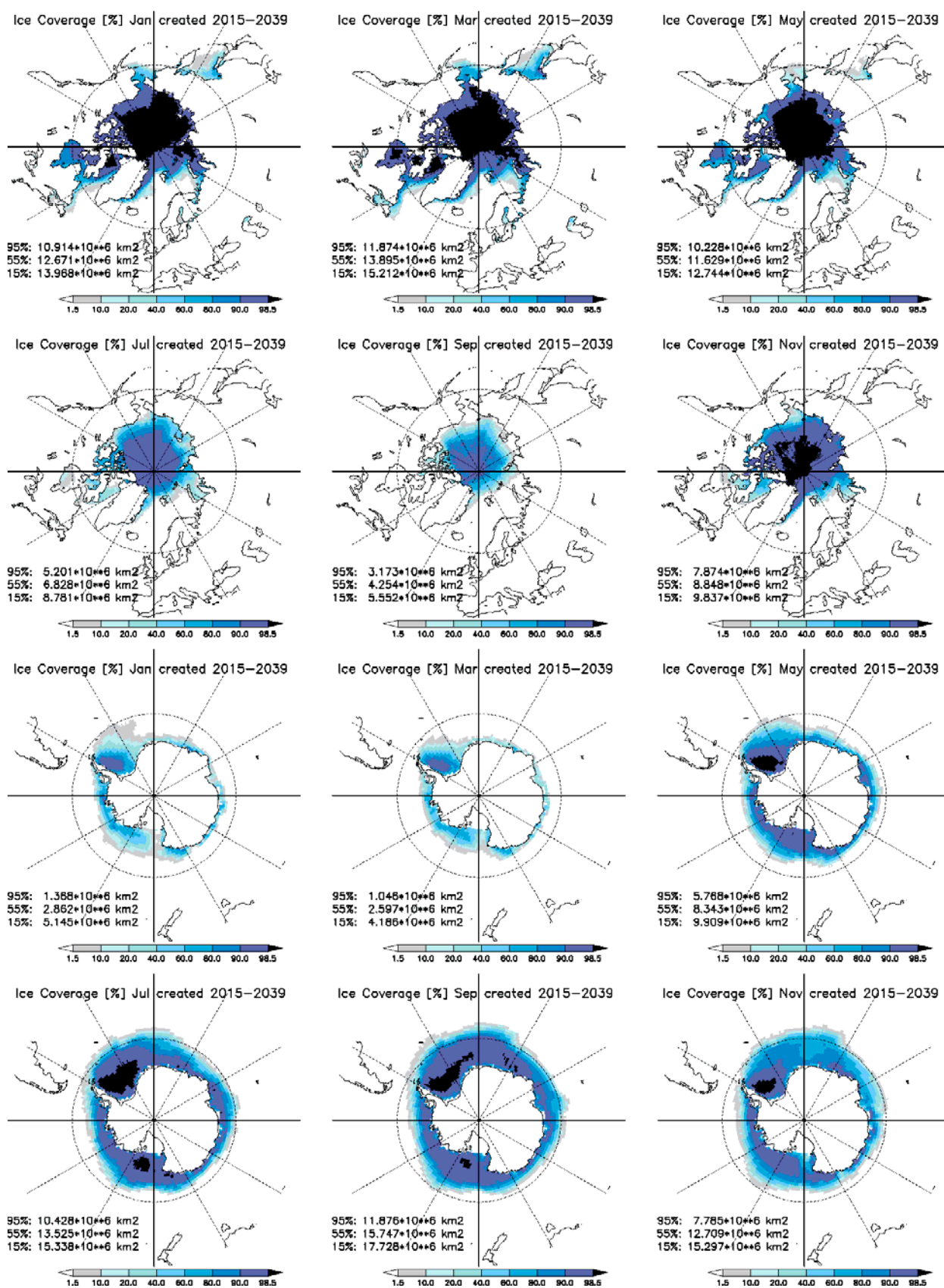


**Fig. S10:** Estimated near-future distributions of monthly sea ice concentrations averaged from 2015 to 2039. The values in the figure denote the sea ice extent for  $f = 95\%$ ,  $55\%$ , and  $15\%$ .

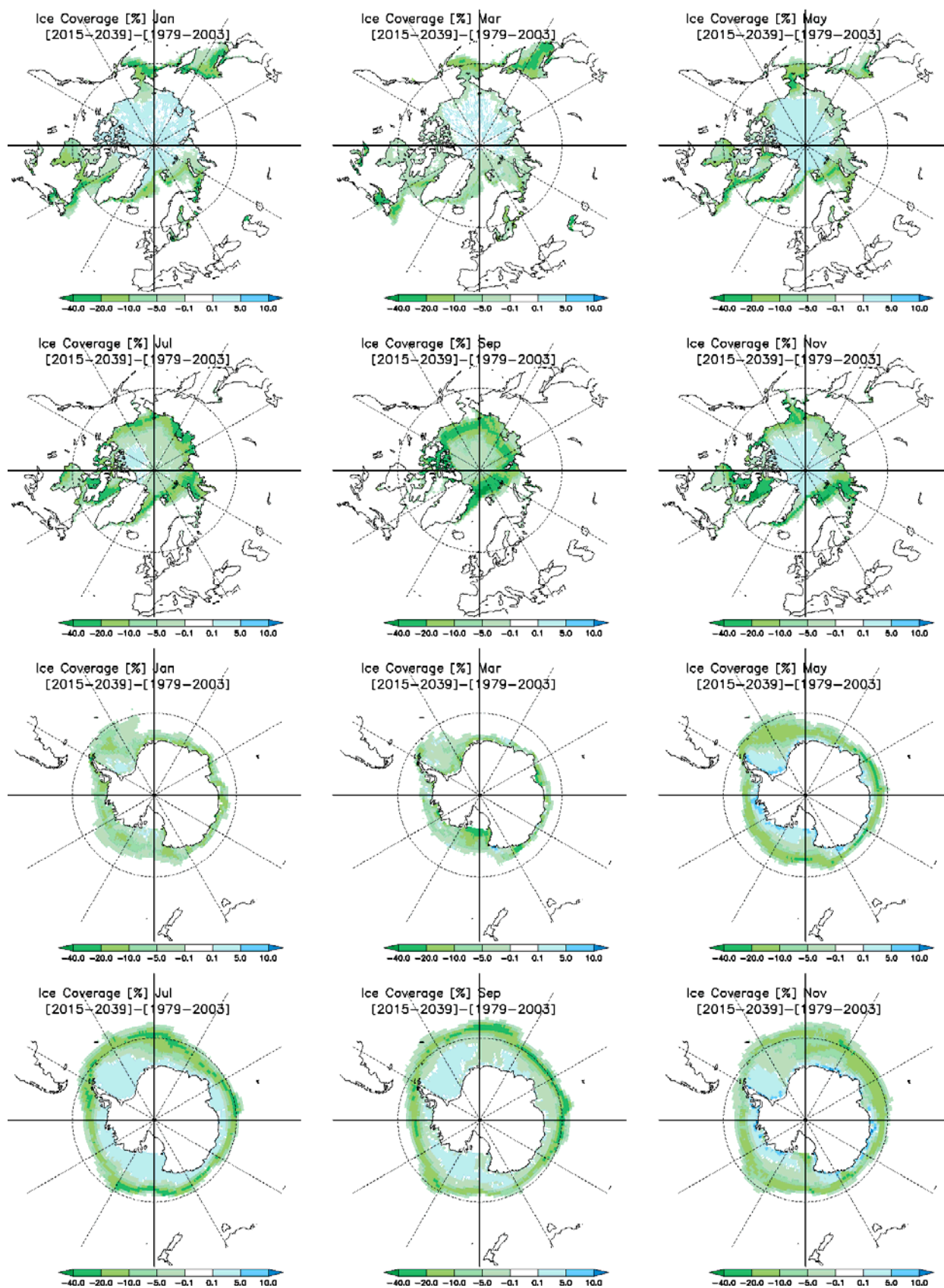


**Fig. S11:** Differences in monthly sea ice concentrations between the observation data (1979–2003) and the estimated near-future values (2015–2039).

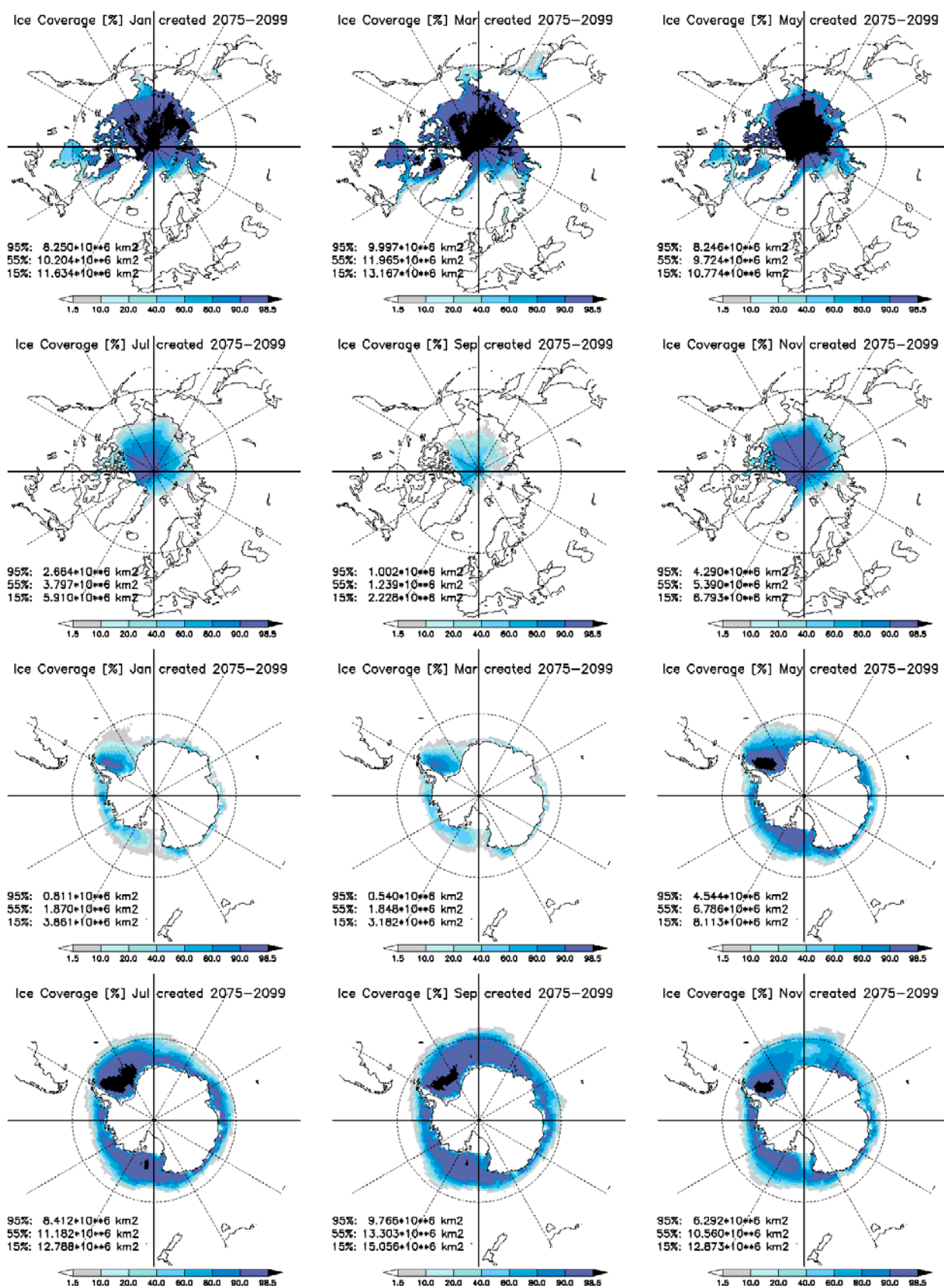


**Fig. S12:** Estimated future distributions of monthly sea ice concentrations averaged from 2075 to 2099. The values in the figure denote the sea ice extent for  $f = 95\%$ ,  $55\%$ , and  $15\%$ .

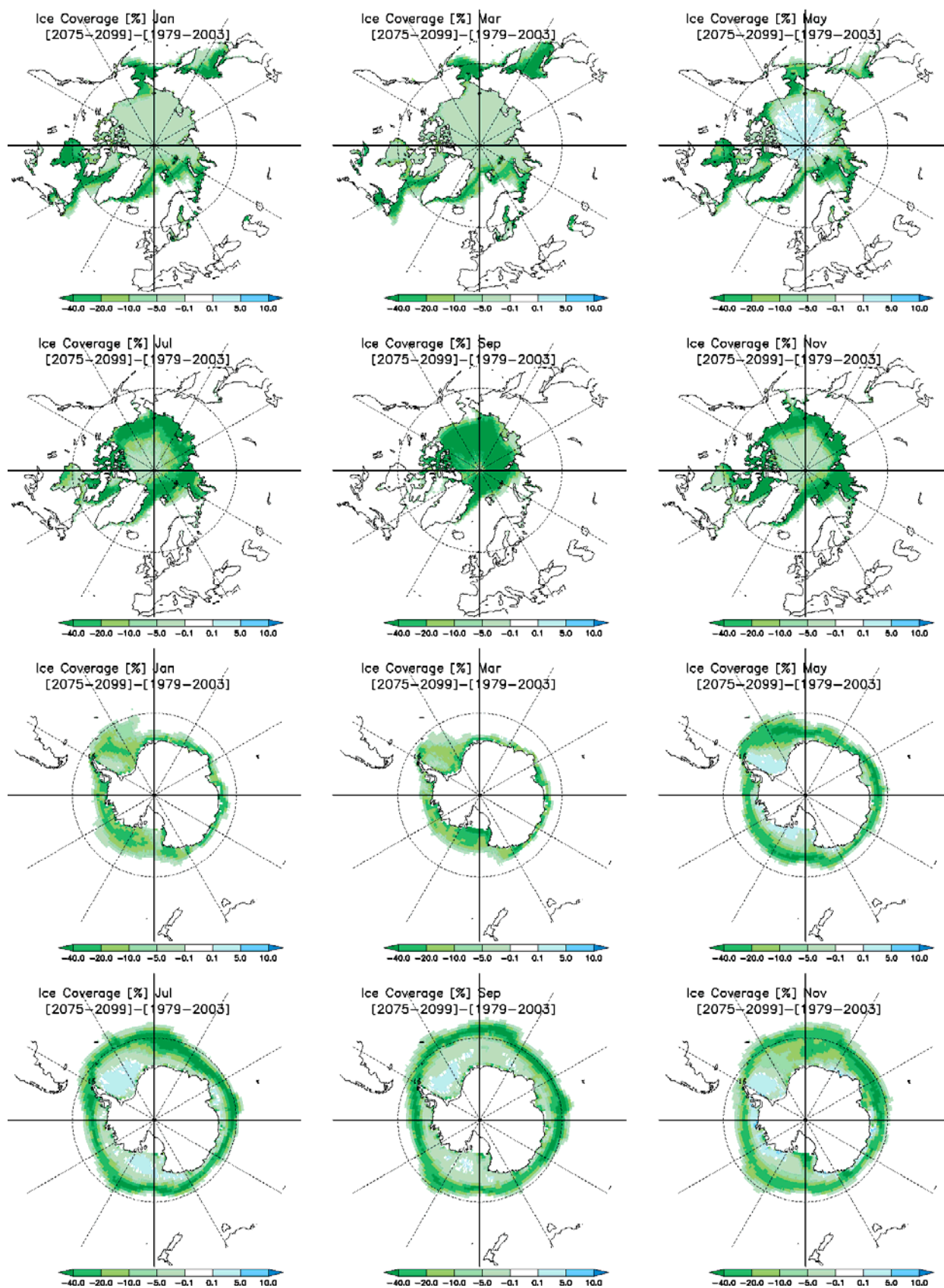


**Fig. S13:** Differences in monthly sea ice concentrations between the observation data (1979–2003) and the estimated future values (2075–2099).

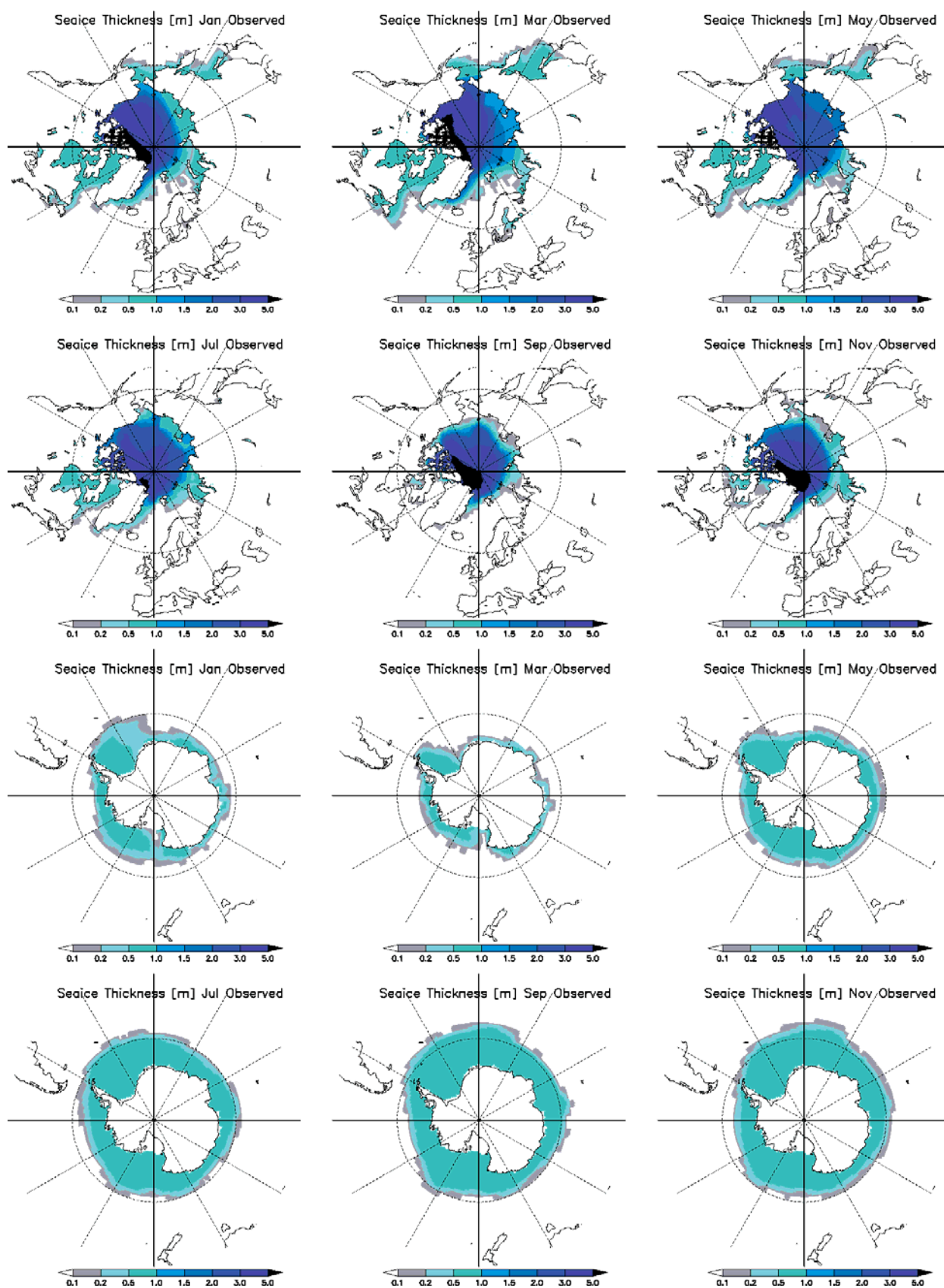
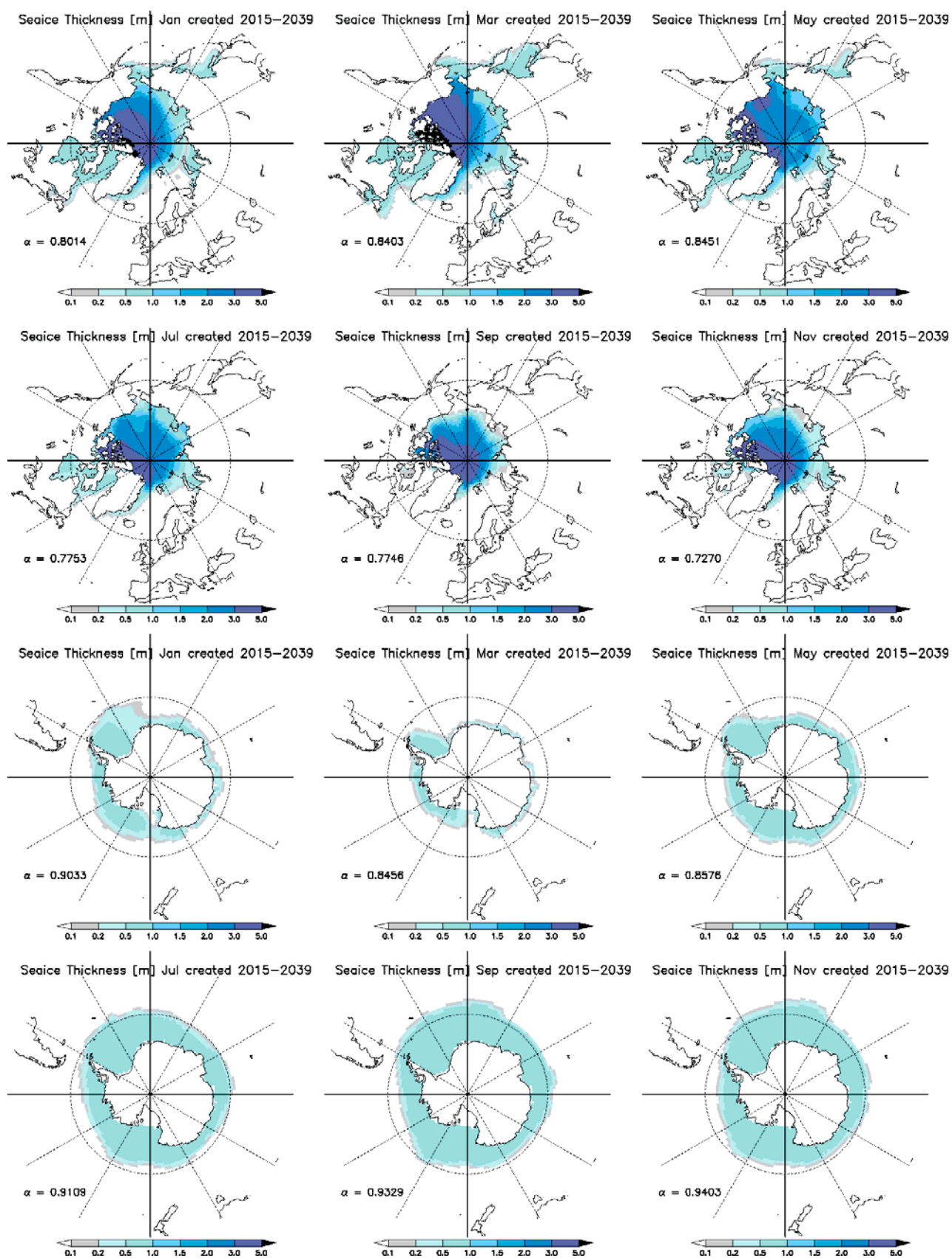
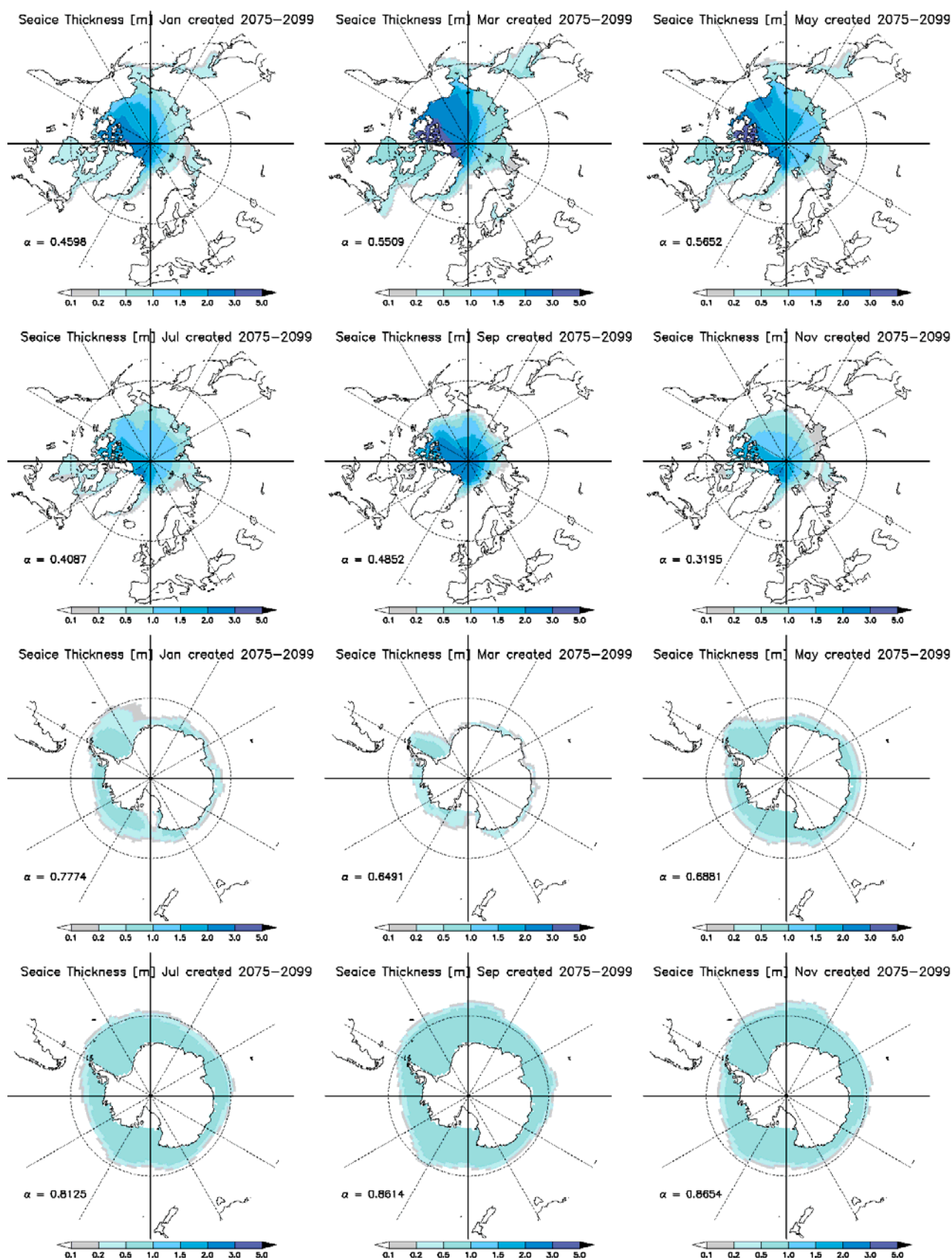


Fig. S14: Observational distributions of monthly sea ice thickness.



**Fig. S15:** Estimated near-future (2015–2039) distributions of monthly sea ice thickness. The values of  $\alpha$  calculated by Eq. (10) are shown.



**Fig. S16:** Estimated future (2075–2099) distributions of monthly sea ice thickness. The values of  $\alpha$  calculated by Eq. (10) are shown.